

Improved performance of SiC radiation detectors due to optimized ohmic contact electrode by graphene insertion

Yuping Jia^{a,b}, Xiaojuan Sun^{a,b}, Zhiming Shi^{a,b}, Ke Jiang^{a,b}, Tong Wu^{a,b}, Hongwei Liang^c, Xingzhu Cui^d, Wei Lü^{a,e,*}, Dabing Li^{a,b,*}

^a State Key Laboratory of Luminescence and Applications, Changchun Institute of Optics, Fine Mechanics and Physics, Chinese Academy of Sciences, Changchun 130033, China

^b Center of Materials Science and Optoelectronics Engineering, University of Chinese Academy of Sciences, Beijing 100049, China

^c School of Microelectronics, Dalian University of Technology, Dalian 116024, China

^d Institute of High Energy Physics, Chinese Academy of Sciences, Beijing 100049, China

^e Key Laboratory of Advanced Structural Materials, Ministry of Education & Advanced Institute of Materials Science, Changchun University of Technology, Changchun 130012, China

ARTICLE INFO

Keywords:

Silicon carbide
Radiation detector
Graphene
Energy resolution

ABSTRACT

SiC as a typical wide bandgap semiconductor has exhibited potential application in alpha particle detectors. However, due to the comparatively high annealing temperature required for traditional fabrication technique of ohmic electrode, it is easy to excite impurities in the SiC epilayer, which act as scattering centers result in the declined device performance. In present work, a graphene layer is inserted between metal ohmic electrode and SiC. The graphene promotes the formation of carbon compounds and thus decreases ohmic contact resistance. Meanwhile, due to the Fermi level adjustable of graphene by external bias, the barrier of interface at graphene insert layer is enlarged at reverse bias. The built-in field accelerates the separation of photo-generated electron-hole pairs. As a result, the graphene inserted device annealed at 400 °C achieved a 3.9%@-40 V energy resolution, and the device even without annealing achieved a 4.4%@-40 V energy resolution for ²³⁹Pu alpha source, which are both better than that of traditional device without graphene layer annealed at 880 °C (6%@-40 V). The detailed mechanism has been discussed and suggested. Present work provides an effective strategy to improve device performance.

1. Introduction

SiC based high resolution semiconductor ionizing radiation detectors have recently attracted great attention due to its unique properties such as high strength, corrosion resistance, chemical inertness, high thermal conductivity, and low thermal expansion coefficient, which makes it an appealing candidate for using in high-temperature and high radiation conditions under which conventional semiconductor detectors cannot adequately perform [1,2]. In particular, SiC epitaxial layer Schottky barrier diodes (SBDs) have established themselves as alpha particle detectors with high-energy resolution [3–5]. Apart from charged particle detection, SiC has been reported to be highly sensitive to ion beam and soft X-ray, and high energy resolution to gamma ray [6–12].

While defect-free high purity single crystals or epitaxial layers are

crucial for SiC radiation detectors with high resolution and high sensitivity, it is still a bottleneck to acquire high quality SiC with carrier density lower than $1 \times 10^{14} \text{ cm}^{-3}$ till now. In addition, high quality ohmic and Schottky contacts are both required to use SiC in semiconductor devices under harsh environments [13–16]. A typical SiC-based detector has a structure of a SBD on the top and a ohmic contact on the bottom as shown in Fig. 1(a) [17]. Due to band alignment, a volume depleted of carriers is created at the semiconductor side of the SBD junction, making the device very sensitive to the presence of electron-hole pairs generated upon illumination with above band-gap light or upon exposure to ionizing radiation. The device is operated under reverse bias, which increases the potential drop across the semiconductor and increases the depletion width. To limit the required operation voltage, the doping level of the substrate is usually two orders

* Corresponding authors at: State Key Laboratory of Luminescence and Applications, Changchun Institute of Optics, Fine Mechanics and Physics, Chinese Academy of Sciences, Changchun 130033, China.

E-mail addresses: lw771119@hotmail.com (W. Lü), lidb@ciomp.ac.cn (D. Li).

<https://doi.org/10.1016/j.diamond.2021.108355>

Received 5 January 2021; Received in revised form 14 March 2021; Accepted 15 March 2021

Available online 22 March 2021

0925-9635/© 2021 Elsevier B.V. All rights reserved.

of magnitude higher than that of the epilayer. Detailed specifications of SiC SBD detectors have been reported elsewhere by several authors using $n-n^+$ structures [18–21].

While Schottky contact and interface between electrode and SiC have been investigated in previous work [22–24], the bottom ohmic contact with low contact resistance is also crucial for efficient signal output. One issue should be addressed is the effect of post-annealing of ohmic electrode on device performance. The temperature of post-annealing is generally higher than 800 °C, which is necessary because the formation of the metal carbide compound during the high temperature annealing results in the low contact resistance [25–27]. However, due to the comparatively high annealing temperature, it is possible to excite impurities in the doped epilayer [28], resulting in the scattering of electrical signal and lowering efficiency of charge collection and energy resolution [29]. For the formation mechanism of ohmic contact between SiC and metal, numerous studies have shown that the graphite transition layer with high carrier concentration and narrow band gap was formed at the metal contact interface, which can reduce the contact barrier [30,31]. For example, the ohmic contact between Ni and n-SiC could be formed after annealing between 900 and 1000 °C [32,33], and M. Said [34] et al. confirmed that a graphite transition layer is formed between Ni and SiC by Raman spectroscopy and X-ray diffraction.

To our best knowledge, post-annealing is still necessary for electrode fabrication till now and there is no alternatively effective method has been reported. Graphene, which structure is two-dimensional sheet of carbon atoms packed in a hexagonal honeycomb lattice, has attracted great attention because of the excellent properties: Dirac Fermions, the extremely high carrier mobility up to $200,000 \text{ cm}^2 \text{ V}^{-1} \text{ s}^{-1}$, large specific surface area of $2630 \text{ m}^2 \text{ g}^{-1}$, Young's modulus of 1.0 TPa, high thermal conductivity of $5300 \text{ W} \cdot \text{m}^{-1} \cdot \text{K}^{-1}$ [35–37]. According to the aforementioned discussion, the advantages of graphene can be used to fabricate high performance SiC radiation detector as the graphite transition layer to optimize ohmic contact. In present work, to improve device performance, a graphene inserted device structure is designed as shown in Fig. 1(b). The graphene film grown on copper foil was transferred to SiC substrate before Ti/Al electrode deposition. For comparison, detectors with and without graphene insertion layer have been fabricated, and the device performances were evaluated.

2. Experiment

2.1. Detector fabrication

In this study, a SiC radiation detector with a $5 \times 10 \text{ mm}^2$ area was fabricated. An image of the device is shown in Fig. 1(c). An illustration of the detector's structure is presented in Fig. 1(b). A $15 \text{ }\mu\text{m}$ epitaxial SiC layer with a n-type doping density of $3.5 \times 10^{14} \text{ cm}^{-3}$ was deposited on an n-doped SiC substrate. A $1 \text{ }\mu\text{m}$ buffer layer with a doping density of $1 \times 10^{18} \text{ cm}^{-3}$ was used between the epitaxial layer and substrate. The epitaxial SiC layer was the alpha particle absorption layer, and the n-doped SiC substrate was used as a conductive layer connected to an ohmic electrode. A 500 nm SiO_2 dielectric layer was deposited between the Schottky electrode and SiC epitaxial layer. The Schottky electrode is made using Ni/Au metal layer with each layer 30 nm thick and annealed at $400 \text{ }^\circ\text{C}$. Here the annealing temperature has been selected according to the experiments as shown in Fig. S1, Supporting information.

The point of present work is to optimize ohmic electrode with graphene layer insertion. Therefore, four devices with different ohmic electrode conditions were fabricated (the surface morphology of Ti/Al/Ti/Au layer with different ohmic electrode conditions are shown in Fig. S2, 1) traditional ohmic electrode without graphene insertion, which is Ti/Al/Ti/Au metal layer with each layer 30 nm thick and annealed at $880 \text{ }^\circ\text{C}$; (2) graphene inserted ohmic electrode between SiC and metal without annealing; (3) graphene inserted ohmic electrode annealed at $400 \text{ }^\circ\text{C}$; (4) graphene inserted ohmic electrode annealed at $880 \text{ }^\circ\text{C}$. The graphene grown on copper foil was transferred on the back of n-SiC substrate before Ti/Al electrode deposition, and the detailed transfer process is shown in Section 2.2.

2.2. Graphene transfer

The graphene transfer process is shown in Fig. 2(a). The graphene film is grown on copper foil using chemical vapor deposition (CVD) method, using methane as carbon source and the hydrogen as protective gas. The polymethyl methacrylate (PMMA) is coated on the top surface of graphene as a protective layer. The copper foil was removed as follows: 1) the PMMA/graphene/Cu/graphene has been wiped off the graphene on another side using oxygen plasma to obtain PMMA/graphene/Cu. 2) the PMMA/graphene/Cu was put on the surface of hydrogen peroxide/hydrochloric acid mixed solution firstly, and then potassium peroxodisulfate solution to remove copper foil. After all the copper has been removed, the PMMA/graphene was transferred onto the

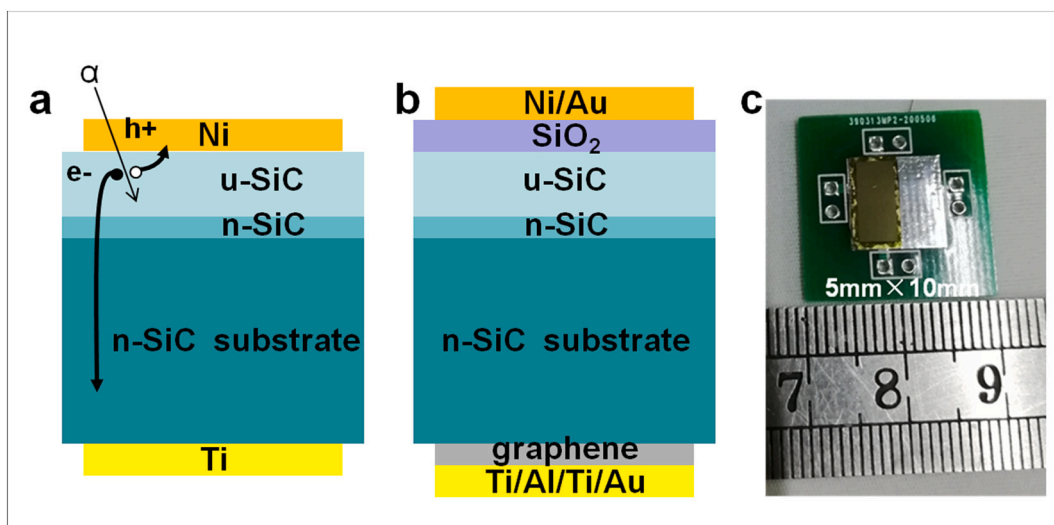


Fig. 1. (a) A schematic diagram of SiC Schottky barrier diode for radiation detection. (b) Illustration of the device's structure. (c) An image of the SiC radiation detector.

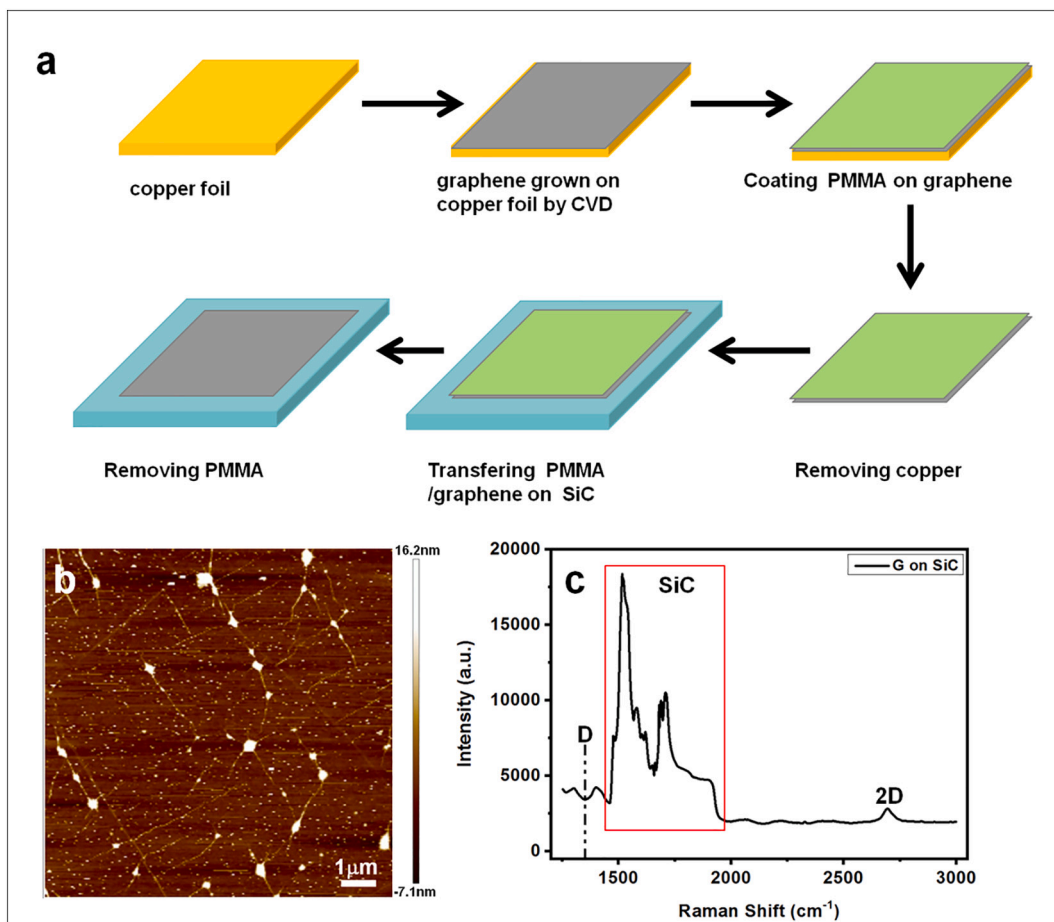


Fig. 2. (a) Illustration of graphene transfer process. (b) AFM image of graphene which has been transferred on SiC. (c) Raman spectra of transferred graphene on SiC.

SiC substrate back surface. At last the PMMA is dissolved by acetone, thus the graphene transfer process is finished.

2.3. Detector characterization

The device was integrated onto a printed circuit board (PCB) board. The Ohmic electrode was directly connected to the center metal pad using silver glue. The Schottky electrode was connected to a side metal pad using an Al wire. A Keithley system was used to measure the device's dark current. Reverse bias was applied to the Schottky electrode. An atomic force microscope (AFM) and scanning electron microscope (SEM) was used to obtain the information of surface morphology. A charge sensitive preamplifier, Gaussian shaping amplifier and a multi-channel analyzer were used to characterize the device's alpha particle detection performance. Because radiation detection is defined as a series of discrete events, the charge amplifier was used as the primary amplification region. The detection signals were low-resistance current pulse signals, and the pulse width was no more than a few ns. For the pre-amplifier, we used a charge-sensitive shaping amplifier that mainly used the feedback capacitance to integrate the input current pulse signals. The output signal was a step signal, while the charge amplifier had a ns rise time signal. Due to the preamplifier's low noise, the signal's electronic noise interference in the system bypass was further reduced. ²³⁹Pu ($E_{\alpha} = 5156.59$ keV) and ²⁴¹Am ($E_{\alpha} = 5485.6$ keV) sources were used to provide α particle irradiation.

3. Results and discussion

Fig. 2(a) is the transfer process of graphene from copper foil to SiC. Preparation of high quality graphene is crucial to promote of the

application of graphene. The main preparation methods of graphene include mechanical exfoliation method, CVD method, reduction of graphene oxide, and organic synthesis method [38–41]. Among them, CVD method could realize graphene preparation of large-scale and high quality. In present, we use CVD method to acquire high quality graphene on copper foil, and transfer it to the surface of SiC with the post transfer procedures as shown in Fig. 2(a). The surface morphology of graphene transferred to SiC is investigated by AFM and shown Fig. 2(b). The continuous film of graphene with numerous wrinkles could be confirmed, and the wrinkles are originated from transfer process. There is no obviously observable damage through AFM image and SEM image as shown in Fig. S3, indicating the excellent property of transferred graphene. Fig. 2(c) is Raman spectra of graphene SiC. According to previous reports, the characteristic D, G and 2D bands of graphene are located around 1345, 1585 and 2696 cm⁻¹, respectively [42]. The D peak is a defect peak. The G and 2D peak are two characteristic peaks of graphene, which can be used to estimate the layer number of graphene. In Fig. 2(c), there is no D band peak could be observed, indicating the excellent quality of transferred graphene. The G peak is submerged in the peak of SiC as marked by red rectangle. The thickness of graphene is ~ 0.68 nm as shown in Fig. S4. However, it should be noticed that several white particles exist on the surface of graphene as shown in Fig. 2(b), Fig. S1 and S5, which is the residual of PMMA and is inevitable due to transfer process. These PMMA particles are most of the shape of ball and the size of them is about 150–400 nm.

The device performances are firstly evaluated by I-V measurement under forward and reverse bias, respectively, which are shown in Fig. 3. Under forward bias as shown in Fig. 3(a), the graphene inserted device without annealing showed the smallest dark current, which is smaller than that of traditional device without graphene layer. The

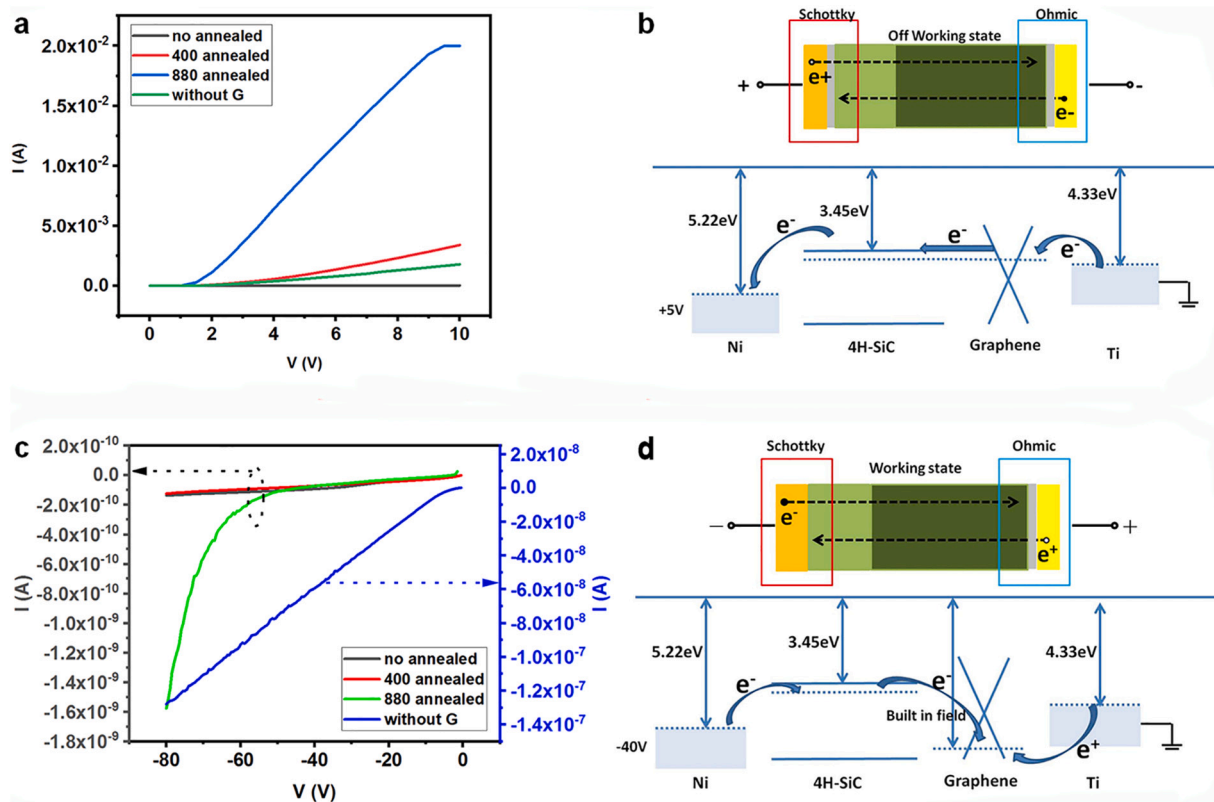


Fig. 3. (a) I-V curves of the devices with and without graphene under different annealing temperatures under forward bias. (b) The working mechanism of device under forward bias. (c) I-V curves of the devices with and without graphene under different annealing temperatures under reverse bias. (d) The working mechanism of device under reverse bias.

corresponding mechanism is shown in Fig. 3(b). As the Fermi level adjustable property of graphene [43–45], the ohmic electrode inject electrons under forward bias condition. As previous studies [25–27,30,31], the formation of the graphite transition layer and carbon compounds at the metal contact interface can reduce the contact barrier. For graphene inserted device without annealing, the barrier height between SiC and metal is not enough effectively adjusted due to the deficiency of high temperature treatment. Therefore, the larger ohmic contact resistance induced the smallest dark current. Due to the insertion of graphene layer, the formation of the graphite transition layer and carbon compounds is easier at 880 °C, which also destroyed the structure of graphene as shown in Fig. S5. As shown Fig. 3(a), it is clear that the forward dark current is increased with the increasing annealing temperature. The 880 °C annealed graphene device shows the largest current. According to the above discussion and results, the ohmic contact resistance is decreased with the increasing annealing temperature under forward voltage.

However, it is different behavior under reverse voltage. As shown in Fig. 3(c), the dark current of the graphene inserted device without annealing is 2 to 3 orders of magnitude lower than that of the traditional device. Since the device is designed to work under reverse bias, the result indicates that the graphene electrode could effectively decrease dark current and thus the device performance is expected to be improved. Under the reverse bias, the ohmic electrode injects holes to graphene, and makes graphene to be p-doped type. As shown in Fig. 3 (d), the two interfaces of SiC/graphene and graphene/metal should be considered respectively. The built-in field formed between graphene and SiC accelerates the electrons transfer from SiC to graphene, promoting the separation of electron-hole pairs. For graphene/metal interface, the barrier formed between graphene and metal under this configuration would inhibit the transfer of electron, and thus the dark current is decreased, which is desired since the device works under reverse bias.

The result indicates both the dark currents of the two graphene inserted devices (without annealing and annealed at 400 °C) can be stabilized below 2×10^{-10} An under 0–80 V bias. For the 880 °C annealed graphene device, the dark current could be maintained below 2×10^{-10} An under 0–60 V. With the further increase in bias to –80 V, the dark current increases sharply to 1.6×10^{-9} A, which is because that the damaged parts of graphene provide current tunneling channels, inducing the increased leakage current.

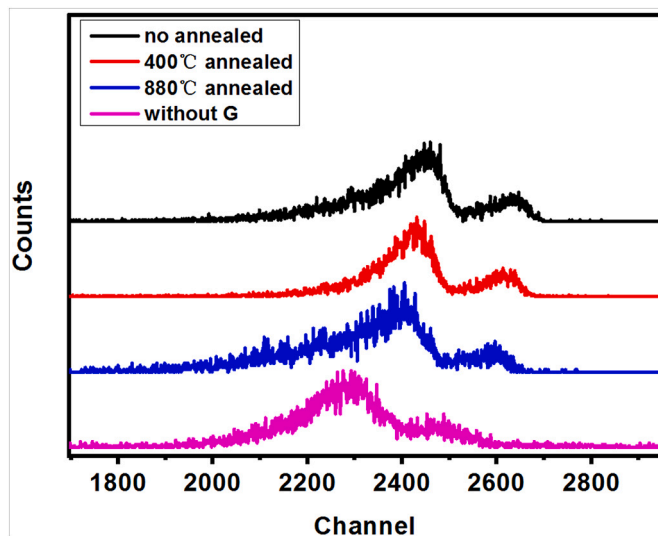


Fig. 4. Pulse height spectra under α irradiation measured in the four detectors at a –40 V bias voltage. The main peak is due to ^{239}Pu radiation and the other peak is corresponding to ^{241}Am .

The detection ability of these detectors was evaluated using α particle radiation detection as shown in Fig. 4, and corresponding parameters of the four devices are shown in Table 1. For all four devices, two peaks could be detected. The main peak is due to ^{239}Pu radiation ($E_{\alpha} = 5156.59$ keV) and the other peak is corresponding to ^{241}Am ($E_{\alpha} = 5485.6$ keV). The peak signals are related to the radiation energy, which was recorded as the channel number by a multichannel analyzer. As shown in Fig. 4, the peak channel number of conventional device is less than those of graphene electrode devices. The peak position of the conventional device is reduced by ~ 150 channels compared with the graphene inserted device without annealing. For devices with graphene electrode, the channel number of peaks decreases with the increasing annealing temperature. Since the number of channels in the multichannel analyzer corresponds to the signal voltage, the more channels, the greater the signal voltage. The larger signal voltage indicates the better charge collection ability of device. Therefore, the graphene electrode can effectively improve the charge collection efficiency. After annealing, the crystallization quality of graphene decreases, and the higher the annealing temperature, the worse the crystallization quality. Therefore, the charge collection efficiency decreases and the peak position moves to the low channel number. The peak position of annealing at $400\text{ }^{\circ}\text{C}$ moves only 16 channels, which indicates that annealing at $400\text{ }^{\circ}\text{C}$ has little effect on the crystallization quality of graphene. It agrees with the results of SEM characterization in Fig. S5. The device annealed at $400\text{ }^{\circ}\text{C}$ achieved the best energy resolution $3.9\%@-40\text{ V}$ among the four devices. The traditional metal electrode without graphene has no built-in electric field, and its charge collection efficiency is lower than that of any devices with graphene. Therefore, the peak position is lower than that of any graphene electrode devices. The dark current results indicate that the traditional devices showed high dark current and low charge collection efficiency, so the energy resolution is poor.

4. Conclusion

In summary, a graphene layer is inserted between metal electrode and SiC to optimize ohmic contact of device in present work. The performances of alpha particle detectors based on graphene electrodes with and without post-annealing have been investigated. We have shown that the graphene inserted electrode can effectively improve the charge collection efficiency. Under working state, a strong built-in electric field would be formed between graphene and SiC and promotes carrier separation upon radiation. The device annealed at $400\text{ }^{\circ}\text{C}$ achieved the best energy resolution $3.9\%@-40\text{ V}$, and the device even without annealing achieved a $4.4\% @-40\text{ V}$ energy resolution. They are both better than that of device without graphene layer annealed at $880\text{ }^{\circ}\text{C}$ ($6\%@-40\text{ V}$). Present work provides an effective strategy to improve device performance.

CRediT authorship contribution statement

Yuping Jia: Experimental Investigation, Methodology, Writing.

Xiaojuan Sun: Data curation, Conceptualization.

Zhiming Shi: Visualization, Investigation.

Ke Jiang: Software.

Tong Wu: Software, Validation.

Hongwei Liang: Data curation, Discussion.

Xingzhu Cui: Investigation.

Wei Lü: Conceptualization, Supervision, Writing- Reviewing and Editing.

Dabing Li: Conceptualization, Supervision, Writing- Reviewing and Editing.

Declaration of competing interest

The authors declare that they have no known competing financial

Table 1

Corresponding parameters of the four devices.

Detector@-40 V	No annealed	400 °C annealed	880 °C annealed	Without G
Peak@ ^{239}Pu	2434	2418	2382	2280
FWHM	106	94	108	136
FWHM%	4.4%	3.9%	4.5%	6%

interests or personal relationships that could have appeared to influence the work reported in this paper.

Acknowledgment

This work was supported by Strategic Priority Research Program of the Chinese Academy of Sciences, Grant No. XDA22020602 and National Natural Science Foundation of China, 61704171, 11705206.

Appendix A. Supplementary data

Supplementary data to this article can be found online at <https://doi.org/10.1016/j.diamond.2021.108355>.

References

- [1] F. Nava, G. Bertuccio, A. Cavallini, E. Vittone, Silicon carbide and its use as a radiation detector material, *Meas. Sci. Technol.* 19 (2008) 102001.
- [2] A. Burger, K.C. Mandal, L.A. Franks, R. Krishna, P.G. Muzykov, R.B. James, Z. Laney, S. Das, T.S. Sudarshan, Radiation Detectors Based on 4H Semi-insulating Silicon Carbide 7805, 2010, p. 78050U.
- [3] F. Nava, P. Vanni, M. Bruzzi, S. Lagomarsino, S. Sciortino, G. Wagner, C. Lanzieri, Minimum ionizing and alpha particles detectors based on epitaxial semiconductor silicon carbide, *IEEE. T. Nucl. Sci.* 51 (2004) 238–244.
- [4] S.K. Chaudhuri, K.J. Zavalla, K.C. Mandal, High resolution alpha particle detection using 4H-SiC epitaxial layers: fabrication, characterization, and noise analysis, *Nucl. Instrum. Meth. A.* 728 (2013) 97–101.
- [5] L. Torrisi, V. Havranek, M. Cutroneo, A. Mackova, L. Calcagno, A. Cannavò, A. Torrisi, SiC detector for high helium energy spectroscopy, *Nucl. Instrum. Meth. A* 903 (2018) 309–316.
- [6] G. Bertuccio, R. Casiraghi, F. Nava, Epitaxial silicon carbide for X-ray detection, *IEEE. T. Nucl. Sci.* 48 (2001) 232–233.
- [7] M.J. Bozack, Surface studies on SiC as related to contacts, *Phys. Status Solidi B* 202 (2015) 549–580.
- [8] J. Crofton, L.M. Porter, J.R. Williams, The physics of ohmic contacts to SiC, *Phys. Status Solidi B* 202 (2015) 581–603.
- [9] A. Sciuto, G. D'Arrigo, S. Di Franco, M. Mazzillo, G. Franzò, L. Torrisi, L. Calcagno, 4H-SiC detector in high photons and ions irradiation regime, *IEEE Trans. Electron Devices* 65 (2018) 599–604.
- [10] D. Margarone, J. Krasa, L. Giuffrida, A. Picciotto, L. Torrisi, T. Nowak, P. Musumeci, A. Velyhan, J. Prokupek, L. Laska, T. Mocek, J. Ullschmied, B. Rus, Full characterization of laser-accelerated ion beams using Faraday cup silicon carbide, and single-crystal diamond detectors, *J. Appl. Phys.* 109 (2011) 103302.
- [11] L. Torrisi, A. Sciuto, A. Cannavò, S. Di Franco, M. Mazzillo, P. Badalà, L. Calcagno, SiC detector for sub-MeV alpha spectrometry, *J. Electron. Mater.* 46 (2017) 4242–4249.
- [12] A. Torrisi, P.W. Wachulak, H. Fiedorowicz, L. Torrisi, Monitoring of the plasma generated by a gas-puff target source, *Phys Rev Accel Beams* 22 (2019), 052901.
- [13] A. Itoh, H. Matsunami, Analysis of Schottky barrier heights of metal/SiC contacts and its possible application to high-voltage rectifying devices, *Phys. Status Solidi A* 162 (2015) 389–408.
- [14] A. Sciuto, L. Torrisi, A. Cannavò, M. Mazzillo, L. Calcagno, Advantages and limits of 4H-SiC detectors for high- and low-flux radiations, *J. Electron. Mater.* 46 (2017) 6403–6410.
- [15] F.L. Via, F. Roccaforte, A. Makhtari, V. Raineri, P. Musumeci, L. Calcagno, Structural and electrical characterisation of titanium and nickel silicide contacts on silicon carbide, *Microelectron. Eng.* 60 (2002) 269–282.
- [16] T. Nakamura, T. Miyonagi, H. Tsuchida, I. Kamata, T. Jikimoto, K. Izumi, Improvement in electrical performance of Schottky contacts for high-voltage diode, *Mater. Sci. Forum* 483–485 (2005) 721–724.
- [17] J. Coutinho, V.J.B. Torres, I. Capan, T. Brodar, Z. Ereš, R. Bernat, V. Radulović, K. Ambrožič, L. Snoj, Z. Pastuović, A. Sarbutt, T. Ohshima, Y. Yamazaki, T. Makino, Silicon carbide diodes for neutron detection, *Nucl. Instrum. Meth. A.* 986 (2021) 164793.
- [18] G. Lioliou, H.K. Chan, T. Gohil, K.V. Vassilevski, N.G. Wright, A.B. Horsfall, A. M. Barnett, 4H-SiC Schottky diode arrays for X-ray detection, *Nucl. Instrum. Meth. A.* 840 (2016) 145–152.
- [19] A.R. Dulloo, F.H. Ruddy, J.G. Seidel, J.M. Adams, J.S. Nico, D.M. Gilliam, The thermal neutron response of miniature silicon carbide semiconductor detectors, *Nucl. Instrum. Meth. A.* 498 (2003) 415–423.

- [20] F. Nava, G. Wagner, C. Lanzieri, P. Vanni, E. Vittone, Investigation of Ni/4H-SiC diodes as radiation detectors with low doped n-type 4H-SiC epilayers, *Nucl. Instrum. Meth. A.* 510 (2003) 273–280.
- [21] R.W. Flammang, J.G. Seidel, F.H. Ruddy, Fast neutron detection with silicon carbide semiconductor radiation detectors, *Nucl. Instrum. Meth. A.* 579 (2007) 177–179.
- [22] F. Roccaforte, F. La Via, V. Raineri, P. Musumeci, L. Calcagno, G.G. Condorelli, Highly reproducible ideal SiC Schottky rectifiers: effects of surface preparation and thermal annealing on the Ni/6H-SiC barrier height, *Appl. Phys. A Mater. Sci. Process.* 77 (2003) 827–833.
- [23] R. Aiba, K. Matsui, M. Baba, S. Harada, H. Yano, N. Iwamuro, Demonstration of superior electrical characteristics for 1.2 kV SiC Schottky barrier diode-wall integrated trench MOSFET with higher Schottky barrier height metal, *IEEE Electron Device Lett.* 41 (2020) 1810–1813.
- [24] M.G. Rastegaeva, A.N. Andreev, A.A. Petrov, A.I. Babanin, M.A. Yagovkina, I. P. Nikitina, The influence of temperature treatment on the formation of Ni-based Schottky diodes and ohmic contacts on 6H-SiC, *Mater. Sci. Eng. B* 46 (1997) 254–258.
- [25] S.Y. Han, K.H. Kim, J.K. Kim, H.W. Jang, K.H. Lee, N.-K. Kim, E.D. Kim, J.-L. Lee, Ohmic contact formation mechanism of Ni on n-type 4H-SiC, *Appl. Phys. Lett.* 79 (2001) 1816–1818.
- [26] Y. Zhang, T. Guo, X. Tang, J. Yang, Y. He, Y. Zhang, Thermal stability study of n-type and p-type ohmic contacts simultaneously formed on 4H-SiC, *J. Alloys Compd.* 731 (2018) 1267–1274.
- [27] V. Van Cuong, S. Ishikawa, T. Maeda, H. Sezaki, S. Yasuno, T. Koganezawa, T. Miyazaki, S.-I. Kuroki, High-temperature reliability of Ni/Nb ohmic contacts on 4H-SiC for harsh environment applications, *Thin Solid Films* 669 (2019) 306–314.
- [28] A.A. Oleg, M.S. Alexander, A.I. Denis, V.M. Alexander, B.V. Andrey, Temperature dependence simulation of electrophysical properties of silicon carbide, in: *The Third International EuroConference on Advanced Semiconductor Devices and Microsystems*, Smolenice Castle, 2000.
- [29] F. Nava, G. Bertuccio, A. Cavallini, E. Vittone, Silicon carbide and its use as a radiation detector material, *Meas. Sci. Technol.* 19 (2008) 102001.
- [30] I.P. Nikitina, K.V. Vassilevski, N.G. Wright, A.B. Horsfall, A.G. O'Neill, C. M. Johnson, Formation and role of graphite and silicide in nickel based ohmic contacts to n-type silicon carbide, *J. Appl. Phys.* 97 (2005) 083709.
- [31] F. Liu, B. Hsia, C. Carraro, A.P. Pisano, R. Maboudian, Enhanced ohmic contact via graphitization of polycrystalline silicon carbide, *Appl. Phys. Lett.* 97 (2010) 262107.
- [32] F. Roccaforte, F.L. Via, V. Raineri, L. Calcagno, P. Musumeci, Improvement of high temperature stability of nickel contacts on n-type 6H-SiC, *Appl. Surf. Sci.* 184 (2001) 295–298.
- [33] P. Machac, B. Barda, J. Maixner, Structural characterization of nickel-titanium film on silicon carbide, *Appl. Surf. Sci.* 254 (2008) 1691–1693.
- [34] M. Siad, M. Abdesslam, A.C. Chami, Role of carbon in the formation of ohmic contact in Ni/4H-SiC and Ni/Ti/4H-SiC, *Appl. Surf. Sci.* 258 (2012) 6819–6822.
- [35] K.I. Bolotin, K.J. Sikes, Z. Jiang, M. Klima, G. Fudenberg, J. Hone, P. Kim, H. L. Stormer, Ultrahigh electron mobility in suspended graphene, *Solid State Commun.* 146 (2008) 351.
- [36] J. Hun Seol, I. Jo, Arden L. Moore, L. Lindsay, Z.H. Aitken, M.T. Pettes, X. Li, Z. Yao, R. Huang, D. Broido, N. Mingo, R.S. Ruoff, L. Shi, Two-dimensional phonon transport in supported graphene, *Science* 328 (2010) 213.
- [37] K.S. Novoselov, A.K. Geim, S.V. Morozov, D. Jiang, Y. Zhang, S.V. Dubonos, I. V. Grigorieva, A.A. Firsov, Electric field effect in atomically thin carbon films, *Science* 306 (2004) 666–669.
- [38] Z.H. Ni, H.M. Wang, J. Kasim, H.M. Fan, T. Yu, Y.H. Wu, Y.P. Feng, Z.X. Shen, Graphene thickness determination using reflection and contrast spectroscopy, *Nano Lett.* 7 (2007) 2758–2763.
- [39] X. Li, W. Cai, J. An, S. Kim, J. Nah, D. Yang, R. Piner, A. Velamakanni, I. Jung, E. Tutuc, S.K. Banerjee, L. Colombo, R.S. Ruoff, Large-area synthesis of high-quality and uniform graphene films on copper foils, *Science* 324 (2009) 1312–1314.
- [40] V.C. Tung, M.J. Allen, Y. Yang, R.B. Kaner, High-throughput solution processing of large-scale graphene, *Nat. Nanotechnol.* 4 (2009) 25–29.
- [41] C.E. Hamilton, J.R. Lomeda, Z.Z. Sun, J.M. Tour, A.R. Barron, High-yield organic dispersions of unfunctionalized graphene, *Nano Lett.* 9 (2009) 3460–3462.
- [42] A.C. Ferrari, J.C. Meyer, V. Scardaci, C. Casiraghi, M. Lazzeri, F. Mauri, S. Piscanec, D. Jiang, K.S. Novoselov, S. Roth, A.K. Geim, Raman spectrum of graphene and graphene layers, *Phys. Rev. Lett.* 97 (2006) 187401.
- [43] J. Yan, Y. Zhang, P. Kim, A. Pinczuk, Electric field effect tuning of Electron-phonon coupling in graphene, *Phys. Rev. Lett.* 98 (2007) 166802.
- [44] H. Zhong, Z.i Liu, G. Xu, Y. Fan, J. Wang, X. Zhang, L. Liu, K. Xu, H. Yang, Self-adaptive electronic contact between graphene and semiconductors, *Appl. Phys. Lett.* 100 (2012) 122108.
- [45] A. Das, S. Pisana, B. Chakraborty, S. Piscanec, S.K. Saha, U.V. Waghmare, K. S. Novoselov, H.R. Krishnamurthy, A.K. Geim, A.C. Ferrari, A.K. Sood, Monitoring dopants by Raman scattering in an electrochemically top-gated graphene transistor, *Nat. Nanotechnol.* 3 (2008) 210.